Science and Technology Indonesia
e-ISSN:2580-4391 p-ISSN:2580-4405
Vol. 11, No. 3, July 2026

Research Paper

Physicochemical Properties and Water Filtration Performance of Electric Field Fabricated Polyvinylidene Fluoride Membranes

Aneka Firdaus[1], Agung Mataram[1*], Rahma Dani[2], Muhammad Satya Putra Gantada[1], Nukman[1], Irwin Bizzy[1], Ahmad Fauzi Ismail[3]

[1]*Department of Mechanical Engineering, Faculty of Engineering, Universitas Sriwijaya, South Sumatera, 30139, Indonesia*
[2]*Department of Physics Education, Faculty of Teacher Training and Education, Universitas Sriwijaya, South Sumatera, 30139, Indonesia*
[3]*Advanced Membrane Technology Research Centre (AMTEC), Faculty of Chemical and Energy Engineering, Universiti Teknologi Malaysia, Johor, 81310, Malaysia*
*__Corresponding author__: amataram@unsri.ac.id

Abstract
This study investigated the use of an electric field-assisted phase inversion method (15 kV) to tailor the properties of PVDF membranes with a thickness of 3 mm. The electric field significantly altered membrane formation, producing porous structures compared to the dense morphology of untreated membranes. Increasing the PVDF concentration (25–35%) reduced the pore size from 11.54 μm to 5.27 μm, resulting in more uniform structures. Surface analysis indicated that the membranes remained relatively smooth, with smaller surface features at higher polymer concentrations. The mechanical properties improved substantially, with the tensile strength increasing from 12.28 MPa to 43.21 MPa and higher stiffness observed. FTIR results revealed enhanced β-phase formation under the electric field, indicating improved chain alignment, supported by increased crystallinity from XRD. In terms of filtration performance, the permeability reached 55.32 L/m^2·h·bar, while turbidity rejection exceeded 90% for all treated membranes. These results demonstrate a promising approach for high-performance PVDF membranes and strong potential as composite base materials.

Keywords
Crystallinity, Filtration, Mechanical, Morphology, Permeability

Received: 20 January 2026, Accepted: 29 March 2026
https://doi.org/10.26554/sti.2026.11.3.808-826

1. INTRODUCTION

Polyvinylidene fluoride (PVDF) is a semi-crystalline polymer with high chemical stability, thermal resistance, hydrophobic properties, and outstanding piezoelectric and pyroelectric capabilities (Marshall et al., 2021). This combination of characteristics makes PVDF an excellent candidate for a wide range of technological applications, including energy storage, biomedical materials, and filtration (Sriyanti et al., 2024a). In water treatment, PVDF membranes are widely used due to their resistance to solvents, stability across a wide pH range, and ability to maintain mechanical integrity during filtration operations (Acarer-Arat et al., 2024). However, filtration performance is significantly influenced by pore morphology and distribution. Conventional fabrication processes, such as phase inversion without an electric field, often result in non-uniform pores, thereby limiting flux efficiency, selectivity, and fouling resistance (Eniola et al., 2024). Therefore, developing more precise pore-formation techniques is essential for improving the quality of water filtration membranes.

Electric field-based methods offer a new approach for polymer membrane engineering. Applying an electric field during membrane formation can induce dipole orientation and polymer chain reorganization, thereby affecting the morphology, pore homogeneity, and crystal phase ratio (Besghini et al., 2019). The electric field increases chain mobility and creates a more directed solvent migration path, resulting in a more uniform pore distribution and good inter-pore connectivity. Preliminary studies have shown that adjusting electrical parameters, such as the voltage of the electric field, contributes to increased pore formation and reduces flow resistance without decreasing the mechanical strength (Firdaus et al., 2025a; Mataram et al., 2024). Another advantage is the minimal need for additives, resulting in a structure that closely resembles that of pure PVDF with high phase purity. For water filtration applications, strict control of pore size and distribution is important to achieve an optimal balance between permeability, contaminant rejection, and fouling resistance.

Most previous studies have focused on electrospinning techniques or conventional phase inversion approaches (Almafie et al., 2025; Sriyanti et al., 2025). For instance, electrospinning has been widely reported to produce highly porous PVDF nanofiber membranes with enhanced permeability and β-phase dominance; however, this method typically requires

complex setups and suffers from limited control over pore interconnectivity and scalability (Navarro-Tovar et al., 2025). The study by Sriyanti et al. (2024b) investigated the physicochemical and mechanical properties of polyvinylidene fluoride nanofiber membranes synthesized using the electrospinning technique. Nanofiber PVDF produced by electrospinning exhibits a smooth morphology without beads, with a diameter of 230–855 nm, a dominant β phase, and crystallinity of 52.67–58.45%, tensile strength increasing to 6.00 MPa with concentration, and chemical stability. Another study by Almafie et al. (2024) also invetigates PVDF membranes fabricated using electrospinning, this study reports that the membranes has tensile strength of 8.25–15.79 MPa. Both studies showed similarities in the characteristics of the membranes produced; specifically, these membranes had relatively low tensile strengths. This suggests that inadequate mechanical strength remains a persistent and widely reported limitation in membrane fabrication, thereby necessitating the development of more effective strategies to improve mechanical robustness.

Similarly, recent developments in near-field electrospinning and nonsolvent-induced phase separation (NIPS) have enabled more ordered fiber deposition, yet challenges remain in achieving structural uniformity and large-scale production (Albiladi et al., 2023). Basko et al. (2023) study reviews the mechanism of PVDF membrane formation using the nonsolvent-induced phase separation (NIPS) method. Increasing the DMAc concentration increases the pore size (60–150 nm) and permeability (2.8–8 L/m^2·h·bar) with a tensile strength that changes from 9–11 to 6 MPa, whereas the addition of water reduces the pore size (55–25 nm), decreases the permeability (2.8–0.5), and reduces the tensile strength (9–6 MPa). On the other hand, Zhang et al. (2024) reported that conventional nonsolvent-induced phase separation (NIPS) relies primarily on thermodynamic instability and diffusion kinetics, which inherently limit precise control over pore architecture and often result in isotropic structures. Although recent modifications, such as those described in a study by Huang et al. (2024) reported that plasma-assisted NIPS have improved surface functionality, these approaches remain dependent on post-treatment rather than direct manipulation of polymer dynamics during membrane formation. Furthermore, recent studies have emphasized that membrane morphology and performance are highly sensitive to molecular interactions and phase separation pathways; however, these parameters are generally tuned through material composition rather than external field-driven mechanisms (Huang et al., 2025).

Despite these advances, a critical gap remains in the ability to actively control membrane formation through external fields that directly influence polymer dynamics during phase separation. To date, there have been few comprehensive reports on the application of electric fields during the formation of pure PVDF membranes, particularly in relation to their physicochemical properties, crystal structure evolution, and filtration performance. More importantly, the underlying mechanism by which electric fields influence pore growth, α–β phase transformation, and structure–function relationships under realistic filtration conditions remains insufficiently understood. This limitation hinders the optimization of the fabrication parameters and restricts the development of membranes with predictable and high-performance characteristics.

In this context, the present study introduces an electric field-assisted phase inversion strategy that enables the active manipulation of membrane formation via electrostatic interactions, including Coulomb forces and Maxwell stresses. Unlike conventional methods that passively rely on thermodynamic and kinetic factors, this approach directly influences polymer chain orientation and phase separation pathways, leading to anisotropic pore evolution and improved structural control. This mechanism not only differentiates the proposed method from existing electrospinning and NIPS-based techniques but also provides a complementary and scalable route for tailoring membrane morphology. Therefore, this study aims to synthesize PVDF membranes through an electric field-assisted formation method and evaluate their morphology, crystal structure, chemical characteristics, and water filtration performance. The results are expected to advance the fundamental understanding of electric field-driven membrane formation and offer a promising pathway for the development of high-performance water filtration membranes with enhanced permeability–selectivity balance.

2. EXPERIMENTAL SECTION

2.1 Materials

Polyvinylidene fluoride (PVDF, Sigma-Aldrich, Singapore) and dimethylformamide (DMF, CAS 68-12-2, anhydrous, 99.8%) were used as received without further purification.

2.2 Fabrication of Membranes

PVDF membranes were fabricated at three different polymer concentrations (25, 30, and 35 wt.%) in DMF to investigate the effect of polymer content on pore formation. The polymer was dissolved in DMF under continuous stirring at approximately 40°C for 8 h until a homogeneous solution was obtained, ensuring sufficient viscosity to achieve a membrane thickness of approximately 3 mm, after which it was stored in an airtight glass container to prevent solvent evaporation. The solution was then cast onto a copper plate mold, with plaster serving as the mold boundary, followed by exposure to a direct current (DC) electric field of 15 kV for 2 min as part of the deposition process following the previous study Firdaus et al. (2025b). Subsequently, the membranes underwent phase inversion through immersion in water until detachment from the copper plate occurred, and were finally dried at room temperature for 24 h. The overall composition of the prepared membranes is presented in Table 1, and a schematic of the PVDF membrane fabrication experiment is illustrated in Figure 1.

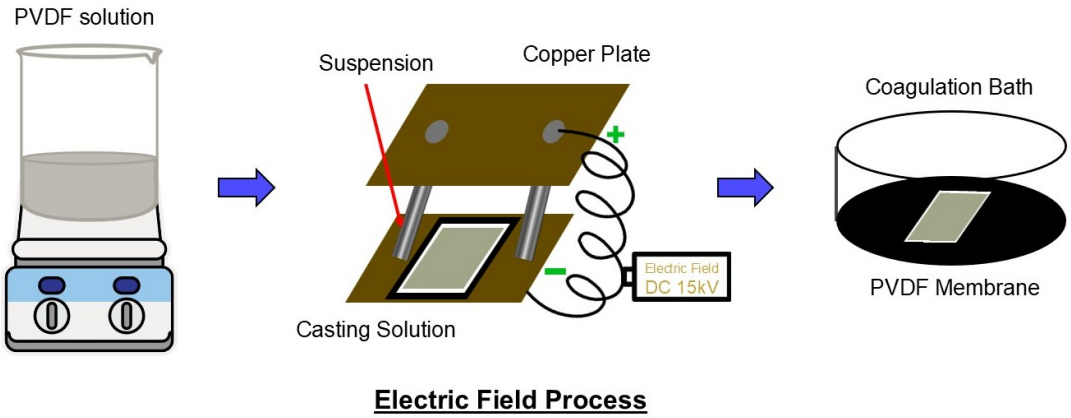

Figure 1. Schematic of Sample Fabrication. Photograph Courtesy of Rahma Dani, copyright 2026.

Table 1. Composition of PVDF Precursor Solution

Sampel	PVDF (g)	Electric Field (kV)
SMP0	25	0
SMP1	25	15
SMP2	30	15
SMP3	35	15

2.3 Characterization

The surface morphology and topographical structure of the membranes were examined using scanning electron microscopy (SEM, Inspect S50, FEI Company) operated at 15 kV after coating the samples with a thin layer of gold to ensure conductivity. Surface roughness and hardness were further analyzed using atomic force microscopy (AFM, AMTEC, UTM) in the three-dimensional mode with a scanning area of 10 × 10 μm. The mechanical properties of the membranes were evaluated through tensile testing using a universal testing machine (ZWICK ROEL Material Testing Machine, Type BT2-FR020TH. A60, Germany) in accordance with the ASTM D638-05 (2008) standard. The crystalline structure of the membranes was characterized using X-ray diffraction (XRD, Rigaku MiniFlex 600, Japan), whereas Fourier-transform infrared spectroscopy (FTIR, Thermo Nicolet iS10, Japan) was employed to identify functional groups and confirm chemical interactions within the PVDF/DMF system. The surface hydrophilicity of the membranes was tested using a digital microscope (Model X4, magnification 1600×). The performance of the membranes was determined through clean water permeability (CWP, Indonesia) testing. Prior to measurement, the membranes were pre-wetted in ultrapure water for 15 min, followed by pressurization at 1–6 bar, and the permeate volume was collected using a 50 mL measuring cylinder for 60 min under standard laboratory conditions (Dani et al., 2026). Turbidity testing was conducted at the Palembang Public Health Laboratory. Wastewater was collected from the river drainage system in Palembang, filtered using a CWP device, and then tested at the Palembang Public Health Laboratory.

3. RESULTS AND DISCUSSION

3.1 Morphology of the PVDF Membranes

Figure 2a shows an SEM image of a PVDF membrane that was not subjected to an electric field (SMP0), while Figures 2b and 2c show membranes subjected to an electric field (SMP1 and SMP3). In general, these observations show that variations in PVDF concentration have a significant impact on the pore size, pore distribution, and density of the resulting membrane structure. SMP1 displays a large pore structure that is unevenly distributed. The presence of these large pores is closely related to the low viscosity of the polymer solution, so that the diffusion rate between the solvent and non-solvent during the electric field process is relatively fast (Hu et al., 2024; Islam et al., 2023). This condition causes the formation of macrovoids, which contribute to increased membrane porosity but can reduce its mechanical stability. In addition, uneven agglomeration is observed on the membrane surface, indicating that the structural stability is not yet optimal at low polymer concentrations.

More importantly, the observed pore formation behavior is strongly governed by the presence of an electric field, as evidenced by SMP0 (without an electric field), which exhibits a dense structure with no observable pores. This confirms that the electric field acts as the primary driving force for pore initiation. Under the applied electric field (SMP1 and SMP3), electrostatic forces, particularly Coulomb forces and Maxwell stress, induce dipole orientation and local deformation within the polymer solution, which accelerates phase separation and promotes the formation of polymer-lean domains that evolve into pores. The presence of large pores in SMP1 (D = 11.54 ± 0.02 μm) indicates that electrostatic forces dominate over viscous resistance, allowing rapid domain growth and expansion. Similar observation have been reported by Ohno et al. (2021) in electric field-assisted PVDF systems, where electrostatic interactions enhance demixing kinetics and promote the

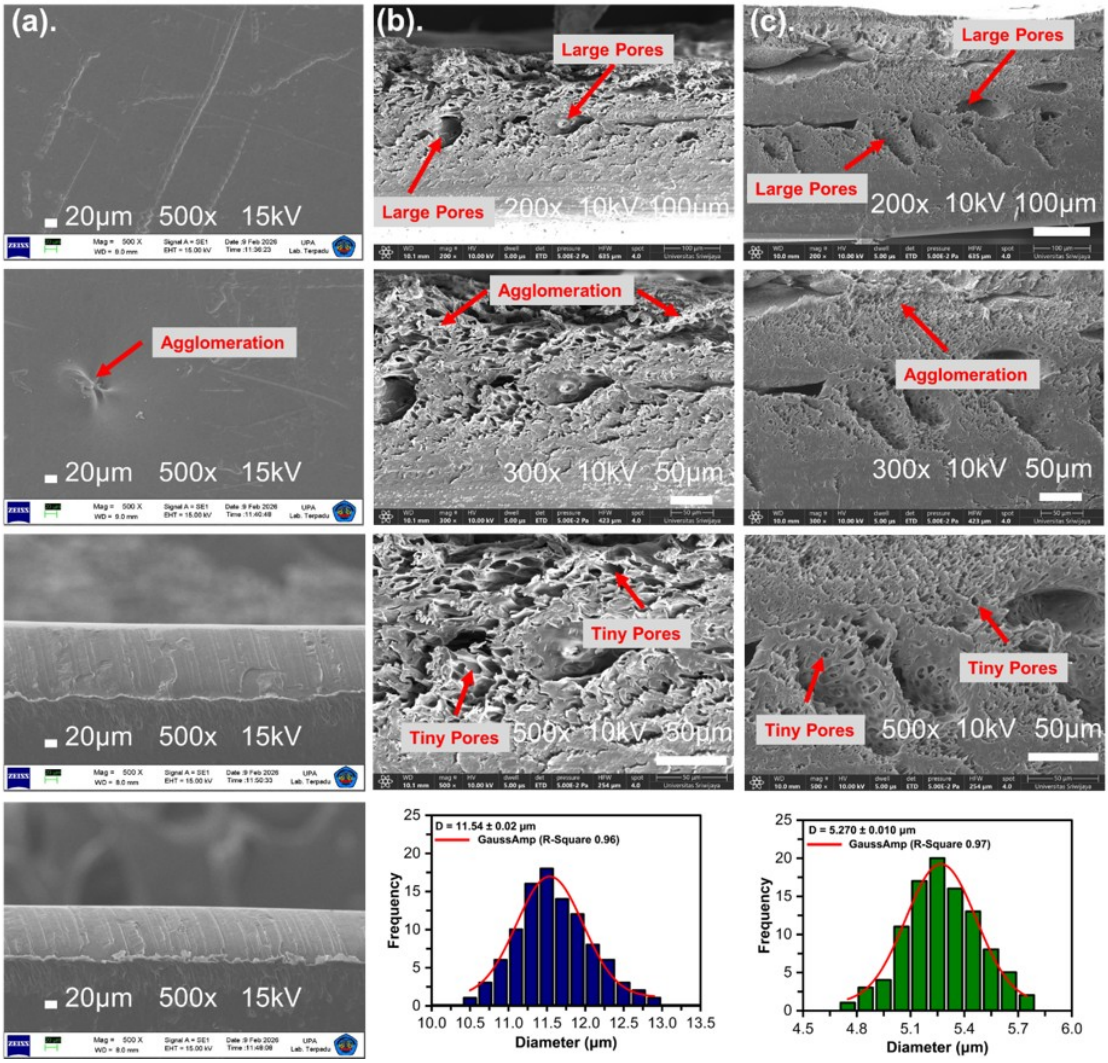

Figure 2. SEM Images and Pores Distribution Graph of the PVDF Membranes (a) SMP0 (b) SMP1 (c) SMP3

formation of more open porous structures.

Conversely, in SMP3, the pore size tends to be smaller with a more homogeneous distribution. This observation is further supported by the pore diameter distribution analysis, where SMP1 exhibited a broader distribution with a larger average diameter (D = 11.54 ± 0.02 μm), indicating structural heterogeneity. In contrast, SMP3 showed a narrower distribution centered at a smaller average diameter (D = 5.27 ± 0.010 μm), reflecting more uniform pore formation. The higher R-square (0.96–0.97) values of the Gaussian fitting in both samples confirmed that the pore size distribution followed a relatively normal trend, with SMP3 demonstrating better uniformity than SMP1. High R^2 values indicated excellent goodness-of-fit between the Gaussian model and experimental data, suggesting that the pore formation process was statistically consistent and reproducible. Furthermore, the slightly higher R^2 value observed in SMP3 implied a narrower deviation from the mean pore size, confirming a more controlled and homogeneous phase separation process than SMP1. In contrast, the broader distribution in SMP1 reflects greater variability in pore growth, which is attributed to the dominance of rapid demixing under lower viscosity conditions (Hamta et al., 2021). This transition from large to small pores under the same electric field strength indicated that pore size was not solely governed by electrostatic forces but rather by the competition between driving and resisting forces. While the electric field provided electrostatic driving forces (Coulomb force and Maxwell stress), the increase in PVDF concentration significantly enhanced viscous and elastic forces owing to chain entanglement, which acted as resisting forces that limited domain growth. Consequently, although pore nucleation still occurred under the electric field, its growth was suppressed, leading to smaller and more uniform pores in SMP3. This mechanism is consistent with recent study by Huang et al. (2025), showing that increasing polymer concentration increases chain entanglement and reduces diffusion rates, thereby producing smaller pore sizes

and denser structures.

The high concentration of PVDF increases the viscosity of the solution, so that the solvent-non-solvent exchange process is slower and more controlled (Bohr et al., 2023; Ghorbandoust et al., 2024). Consequently, the membrane structure becomes denser with uniform micropores. This condition positively impacts the mechanical properties of the membrane because the bonds between the polymer chains are stronger, although it reduces water permeability. SEM images also show that the number of macrovoids is significantly reduced in membranes with high concentrations, indicating a morphological transition from a large porous structure to a denser structure (Gayatri et al., 2024; Qua et al., 2022).

This phenomenon of pore size differences can be explained through thermodynamic mechanisms in phase change processes and the effects of electrical fields. In solutions with low viscosity (SMP1), molecular mobility is higher, so solvents easily diffuse out when they come into contact with non-solvents (Ahmadi Bonakdar and Rodrigue, 2024; Choi et al., 2023). This triggers the formation of a solvent-rich phase, which subsequently collapses to form large pores. Conversely, in solutions with high viscosity (SMP3), molecular mobility is limited, so the demixing process proceeds slowly, resulting in smaller, more uniform pores (Annadurai and Alam, 2025). This behavior is consistent with NIPS-based membrane study by Basko et al. (2023), where pore size is governed by the balance between diffusion kinetics and phase separation rate. Furthermore, other study by Huang et al. (2024) in field-assisted membrane fabrication also demonstrate that external fields can control pore morphology by modifying molecular orientation and interfacial dynamics, leading to tunable pore structures.

In addition to the influence of pore size, the agglomeration observed in both samples indicates the interaction between polymer chains. At low concentrations, agglomeration appears to be more dominant due to the lack of polymer density supporting the membrane structure, resulting in uneven empty areas (Kariuki et al., 2022). At high concentrations, agglomeration tends to decrease because the denser polymer density results in a smoother membrane surface. These results are consistent with previous studies on PVDF-based membranes, where increased polymer concentration is associated with improved structural compactness and surface smoothing (Sriyanti et al., 2024b). However, the trade-off between permeability and mechanical strength remains a key factor to consider in membrane design. Membranes with large pores do offer high water flux, but they are prone to fouling and decreased mechanical stability (Chen et al., 2024b; Sisay et al., 2023). Conversely, membranes with small pores tend to have better stability and mechanical resistance, but their water permeability decreases (Hami et al., 2023). Thus, variations in PVDF concentration and the application of an electric field act synergistically as key parameters in controlling membrane morphology. The electric field initiates pore formation through electrostatic forces, while polymer concentration governs pore size through viscoelastic resistance, resulting in a transition from non-porous (SMP0) to large-pore (SMP1) and finally to compact small-pore structures (SMP3), consistent with trends reported in recent PVDF membrane studies.

3.2 Topography of the PVDF Membranes

Topographic analysis using atomic force microscopy (AFM) revealed significant differences in the surface morphology of PVDF membranes owing to variations in polymer concentration. Figure 3a is an SMP1 image showing a wavy surface landscape with a relatively large peak-to-valley amplitude of >2 μm and an uneven height distribution, reflecting rapid demixing dynamics due to low solution viscosity, which produces large pores up to the surface (Arif et al., 2019; Hu et al., 2024). This high roughness increases the contact area and can increase flux, but it also creates many fouling retention sites and reduces mechanical stability (Nazari and Abdelrasoul, 2022). In contrast, the topography of SMP3, shown in Figure 3b, exhibits a more homogeneous profile with a much lower height amplitude of <1 μm. The transition between peaks and valleys is smooth, and there are indications of structural regularity due to more controlled solvent-non-solvent exchange (Bohr et al., 2023; Ghorbandoust et al., 2024). This surface smoothness strengthens the bonds between polymer chains, increasing mechanical strength and reducing the potential for fouling, although water permeability tends to decrease (Nagandran et al., 2020). The topographical differences between SMP1 and SMP3 also have implications for the nature of the interface. The rough surface of SMP1 reduces the apparent contact angle and increases initial hydrophilicity; however, extreme irregularities can trap particles. Conversely, SMP3 with its smooth texture produces a more even distribution of interfacial tension and minimizes the accumulation of organic fouling (Kim et al., 2025; Sultana et al., 2025). Overall, the AFM results confirm that polymer concentration is a key parameter controlling the evolution of the PVDF surface texture from a wavy topography and high porosity to a smooth and compact morphology, thereby enabling the adjustment of membrane properties according to application requirements.

3.3 Mechanical Properties of PVDF Membranes

The mechanical property testing results of the PVDF membranes, shown in Figure 4, indicate a consistent relationship between the application of an electric field, increasing polymer concentration, and the resulting mechanical performance, which is comprehensively reflected in all parameters, namely, the stress–strain curve, tensile strength, elongation at break, and Young's modulus. In general, an increase in PVDF concentration from 25% (SMP1), 30% (SMP2), to 35% (SMP3) resulted in a significant increase in tensile strength, elasticity, and material stiffness. This study also utilized a benchmark sample in the form of a membrane with a 25% PVDF concentration without electric field treatment (SMP0), aimed at analyzing the effect of applying an electric field on the membrane's mechanical characteristics. Based on the tensile strength graph, the tensile strength value increased from 12.28 MPa in SMP0

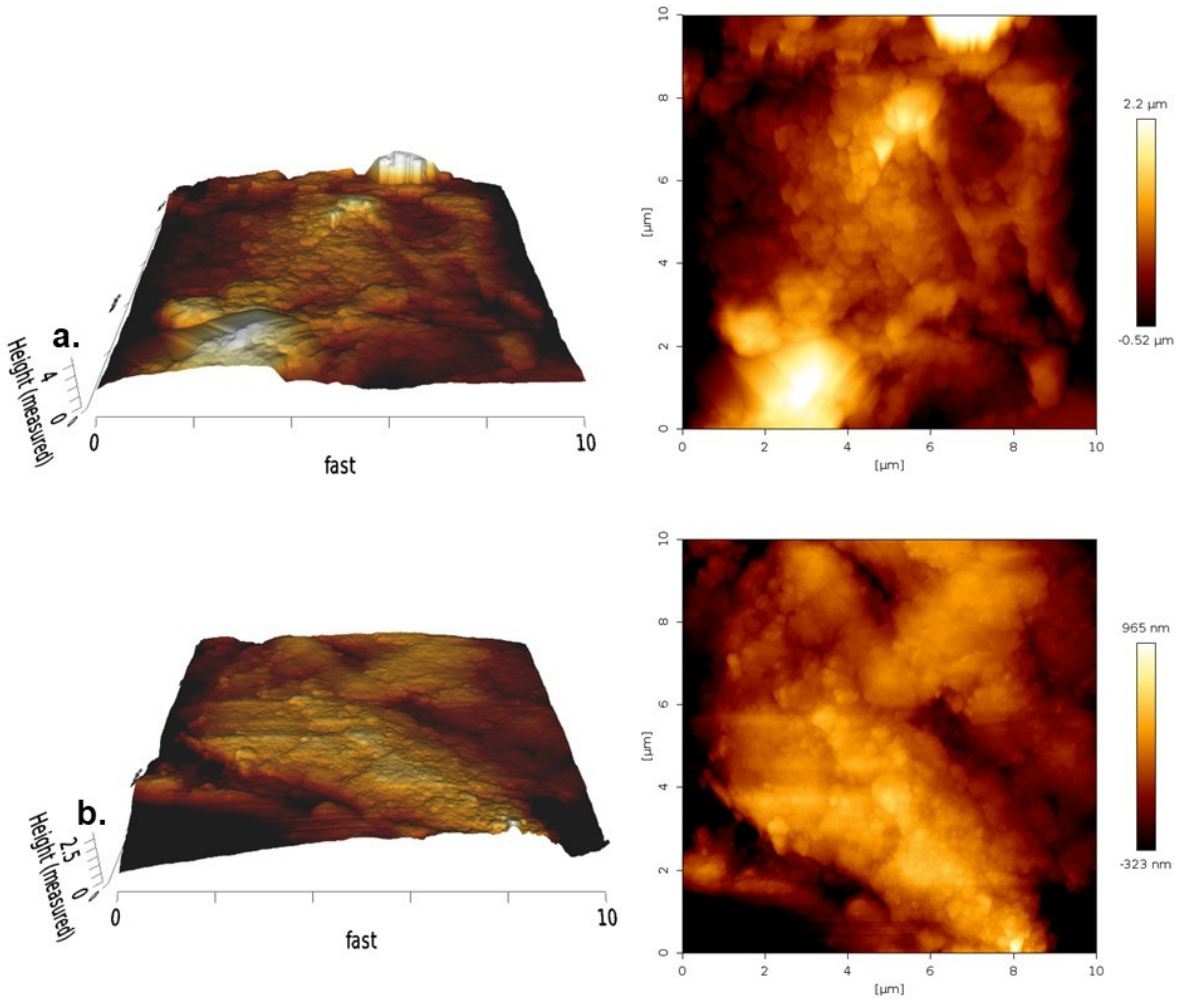

Figure 3. Atomic Force Microscopy Images of the (a) SMP1 and (b) SMP3

to 18.47 MPa in SMP1, 38.28 MPa in SMP2, and reached 43.21 MPa in SMP3. This trend aligns with the stress–strain curve, indicating that samples subjected to an electric field and with higher PVDF concentrations possess a greater ability to withstand stress before failure occurs. This increase indicates that the use of an electric field and higher polymer concentrations results in a denser membrane structure, where interchain polymer interactions become stronger and produce a mechanically more stable network (Marshall et al., 2021; Sriyanti et al., 2024a).

Additionally, the elongation at break graph shows an increase from 6.7% (SMP0) to 10.1% (SMP1), 13.1% (SMP2), and 15.9% (SMP3), indicating that the membrane becomes stronger and more ductile. This result indicates that the application of an electric field and increasing the PVDF concentration do not make the material brittle but rather improve the balance between strength and flexibility. This phenomenon explained by Amin et al. (2023); Osama et al. (2024), by the increased polymer chain density, which allows for a more even distribution of stress during the deformation process, thereby slowing down crack initiation. The correlation between elongation at break and the stress–strain curve is evident, with SMP3 exhibiting a wider curve area, indicating a higher capacity to absorb deformation energy compared to the other samples. Furthermore, the increase in Young's modulus from 350 MPa (SMP1) to 710 MPa (SMP2) and 780 MPa (SMP3) indicates that the membrane becomes stiffer as the PVDF concentration increases. A high Young's modulus indicates that the material has greater resistance to elastic deformation, which is directly correlated with increased tensile strength. Thus, these three parameters (tensile strength, elongation, and modulus) demonstrate a mutually reinforcing relationship: increased PVDF concentration results in a stronger, stiffer membrane while maintaining good deformation capacity (Amin et al., 2023; Osama et al., 2024).

The role of the electric field method in the fabrication process also significantly contributes to the improvement of the membrane's mechanical performance. Compared to SMP0 (without electric field), which exhibits significantly lower tensile strength (10–12 MPa), elongation (6.7%), and modulus (178

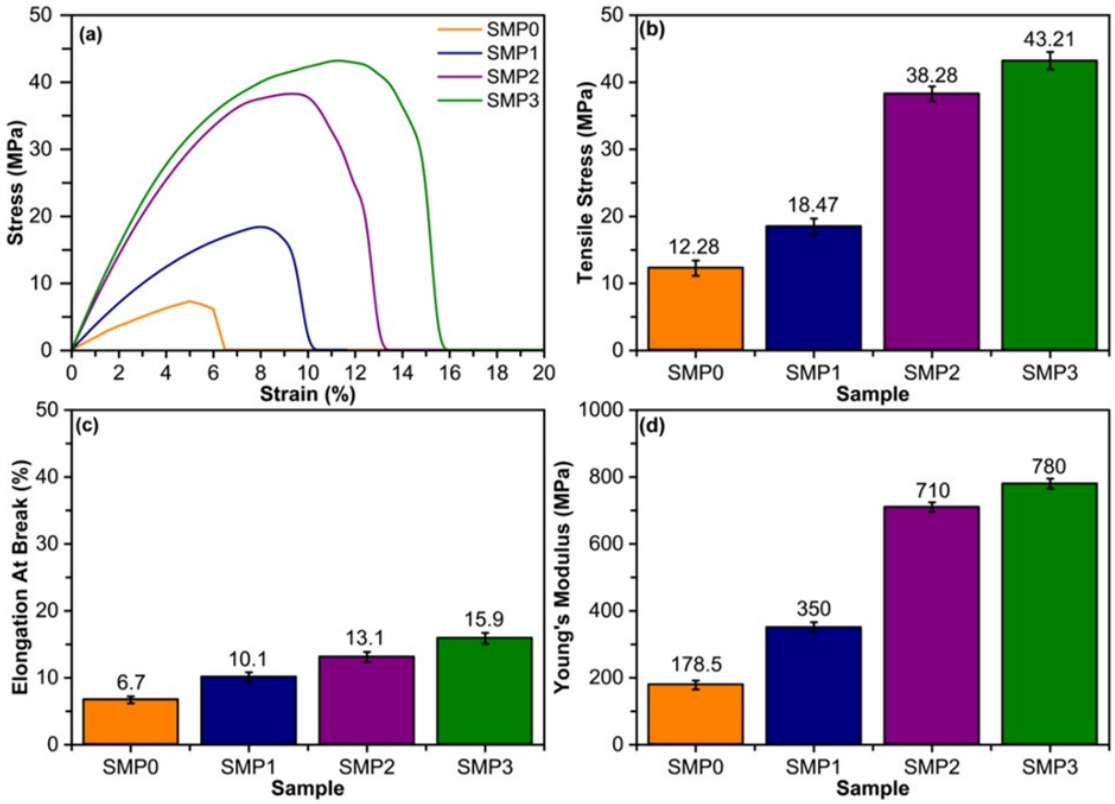

Figure 4. Mechanical Properties of the SMP0, SMP1, SMP2 and SMP3 (a) Strees-Strain Curve (b) Tensile Stress (c) Elongation at Break (d) Young's Modulus

MPa). The application of a DC electric field during the membrane formation process influences the orientation of PVDF molecules, resulting in a more organized structure and a more homogeneous pore distribution. Clearly demonstrates that the application of a DC electric field induces a fundamental transformation in the internal structure of the PVDF membrane.

Mechanistically, this improvement is governed by the interplay of electrostatic forces, primarily Coulomb forces and Maxwell stress as the main driving forces, and viscous as well as elastic forces (arising from chain entanglement) as resisting forces. Under the applied electric field, dipolar PVDF chains experience electrostatic torque and stretching, leading to chain alignment and enhanced molecular orientation. This phenomenon is reported in recent PVDF studies by Tansel (2021); Zhang et al. (2023), where electric field-induced alignment promotes the formation of polar β-phase and significantly enhances mechanical and electromechanical properties.

Furthermore, the contribution of Maxwell stress, which scales with the square of the electric field, induces internal electrostatic pressure that promotes structural densification and chain packing. This electro-mechanical coupling mechanism has been analyzed by Zhang et al. (2025b) this phenomenon been shown to enhance stiffness and strength in PVDF-based systems through electrostriction and dipole alignment effects. In addition, other studies by Fu et al. (2025) on electrically assisted polymer systems report that electric fields facilitate molecular rearrangement and defect minimization, resulting in improved interchain interactions and load transfer efficiency. Similar observations by Qiao et al. (2023) have also been reported in field-assisted orientation systems, where external fields (electric or magnetic) align internal structures and significantly improve mechanical integrity and structural homogeneity.

The progressive increase in tensile strength from SMP1 to SMP3 further indicates that the electric field effect is not isolated but is synergistically enhanced by increasing polymer concentration. While electrostatic forces promote chain alignment, the increased viscosity at higher PVDF concentrations strengthens intermolecular interactions and suppresses chain relaxation, effectively "locking" the oriented structure. This competition between electrostatic driving forces and viscoelastic resisting forces results in a highly compact and homogeneous structure, which improves the stress distribution and reduces localized failure points. Similar synergistic mechanisms between molecular orientation and structural densification have been reported in recent PVDF study by Chen et al. (2024a), where enhanced crystallinity and chain alignment lead to substantial improvements in mechanical performance.

The improvement in mechanical properties from SMP0 to SMP3 is also directly correlated with the effects of the electric

field, porosity, and crystallinity. The application of an electric field during fabrication promotes the orientation of PVDF chains and enhances the formation of crystalline phases (particularly the β-phase), thereby increasing the tensile strength and modulus. Simultaneously, increasing the PVDF concentration reduces porosity and results in a denser, more homogeneous structure, thereby reducing weak points (large voids) and improving mechanical strength. This combination explains the significant increase in tensile strength and Young's modulus, as well as the increase in elongation owing to the more integrated structure.

These results are consistent with a study by He et al. (2022), which reported that an increase in PVDF concentration enhances crystallinity and results in a mechanically stronger structure due to reduced system compatibility and an increased crystallization temperature. In addition, a recent study by Zhang et al. (2025a), shows that increased crystallinity (β-phase) and controlled porosity result in an optimal balance between mechanical strength and membrane structural stability. Thus, the improvement in the mechanical properties of the membrane is primarily driven by the synergy between chain orientation induced by an electric field, reduced porosity, and increased crystallinity.

The correlations among the graphs also indicate that the increase in Young's modulus does not significantly compromise elongation, suggesting that the resulting membrane structure possesses an optimal balance between rigidity and flexibility. This is crucial in membrane applications, where the material must withstand operational pressures without experiencing permanent deformation or structural damage. In other words, increasing the PVDF concentration and applying an electric field creates a synergy that not only enhances tensile strength but also improves overall structural stability (Yang et al., 2025)
.

The error bars presented in (Figure 4b-d) represent the standard deviation of the measurements and provide important insight into the data variability and reproducibility of the mechanical properties. Overall, the relatively small error bars observed across all samples (SMP0–SMP3) indicate good experimental consistency and reliable measurement repeatability. In the tensile strength data (Figure 4b), the narrow error range suggests that the measured values are highly consistent, particularly for SMP2 and SMP3, implying that the enhancement in strength due to the applied electric field is not only significant but also reproducible. In addition, the Young's modulus data (Figure 4d) also exhibit small error bars, especially at higher electric field conditions (SMP2 and SMP3), suggesting that the increased stiffness is consistently achieved. In addition, the Young's modulus data (Figure 4d) also exhibit small error bars, especially at higher electric field conditions (SMP2 and SMP3), suggesting that the increased stiffness is consistently achieved. Overall, the error bar analysis supports the conclusion that the application of an electric field leads to not only enhanced but also highly reproducible mechanical performance.

Overall, these results confirm that increasing the PVDF concentration in combination with electric field techniques is an effective approach for enhancing membrane mechanical properties. Improvements were not limited to a single parameter; all mechanical parameters showed consistent and mutually correlated improvements. This indicates that this method has great potential for the development of high-performance membranes, particularly for applications requiring high mechanical strength and long-term stability. A comparison of the PVDF membrane water flux with that in previous studies is presented in Table 2.

3.4 FTIR Analysis of the PVDF Membranes

The FTIR spectrum of the SMP2 membrane in Figure 5 confirms the chemical integrity of the polymer backbone and reveals the dominance of electroactive crystal motifs relevant to membrane function. The band at 2922 cm^{-1} is consistent with the aliphatic C–H stretching of the CH_2 group, which verifies the preservation of the fluoride vinylidene repeat unit, while the weak absorption near 2360 cm^{-1} is characteristic of atmospheric CO_2 and should be considered an extrinsic artifact rather than a sample feature (Thakur and Han, 2022). In the fingerprint region, clear absorption at 1275 cm^{-1} and 840 cm^{-1} along with supporting features at 1175 and 1072 cm^{-1} are diagnostic of CF_2 and CH_2 vibrations associated with the all-trans (β) conformation of PVDF He et al. (2022). The peak at 1402 cm^{-1} is caused by the CH_2 bending mode and further supports a well-defined crystal lattice (Ke et al., 2020). The minor band at 877 cm^{-1} indicates a minor contribution from other polymorphs (α/γ), implying that the membrane is not in a pure phase but is dominated by the polar β phase (Gayatri et al., 2024).

To further substantiate this observation, a semi-quantitative assessment of the phase composition was performed based on the relative intensities of the characteristic FTIR peaks. The β-phase fraction in PVDF is commonly evaluated by comparing the absorbance of the β-phase band at 840 cm^{-1} with that of the α-phase band at 762–764 cm^{-1}. In the present spectrum, the β-phase peak at 840 cm^{-1} exhibited significantly higher intensity than the α-phase peak at 762 cm^{-1} ($A_{840} \gg A_{762}$) , indicating a high fraction of electroactive β-phase. This approach follows the well-established Gregorio method, which has been widely adopted for semi-quantitative phase analysis in PVDF systems (Roni et al., 2025). The relatively weak α-phase contribution, together with the absence of strong α-characteristic bands, further confirms the suppression of nonpolar crystalline domains.

This result is consistent with recent studies by Bertolini et al. (2023); Zaitzeff and Groven (2023), reporting that enhanced β-phase formation is characterized by dominant absorption bands at 840 and 1275 cm^{-1}, particularly in PVDF membranes processed under external stimuli such as electric fields or controlled crystallization conditions. Similar trends have also been observed in advanced PVDF-based systems studies by Fakhry et al. (2025); Jayasekara and Cebe (2023); Silva et al. (2023), where processing -induced dipole alignment promotes β-phase

Table 2. Comparison of PVDF Membrane Tensile Stress with Previous Studies

Membrane Material	Fabrication Methods	Tensile Stress (MPa)	References
PVDF/GO	Dip Coating Technique Combining nonsolvent-Induced phase	4.97 – 6.15	(Dawam et al., 2025)
PVDF/p-ATP	separation (NIPS) and thermally-induced phase separation (TIPS)	4.4	(Mao et al., 2023)
PVDF/TiO_2	Phase Inversion	~0.93 – ~2.28	(Mao et al., 2023)
PVDF/PANI/GO	Phase Inversion	~1.5 – ~5	(Nawaz et al., 2021)
PAN/PVDF	Electrospinning	8.25	(Almafie et al., 2024)
PVDF	Electric Field	18.47 – 43.21	This Study

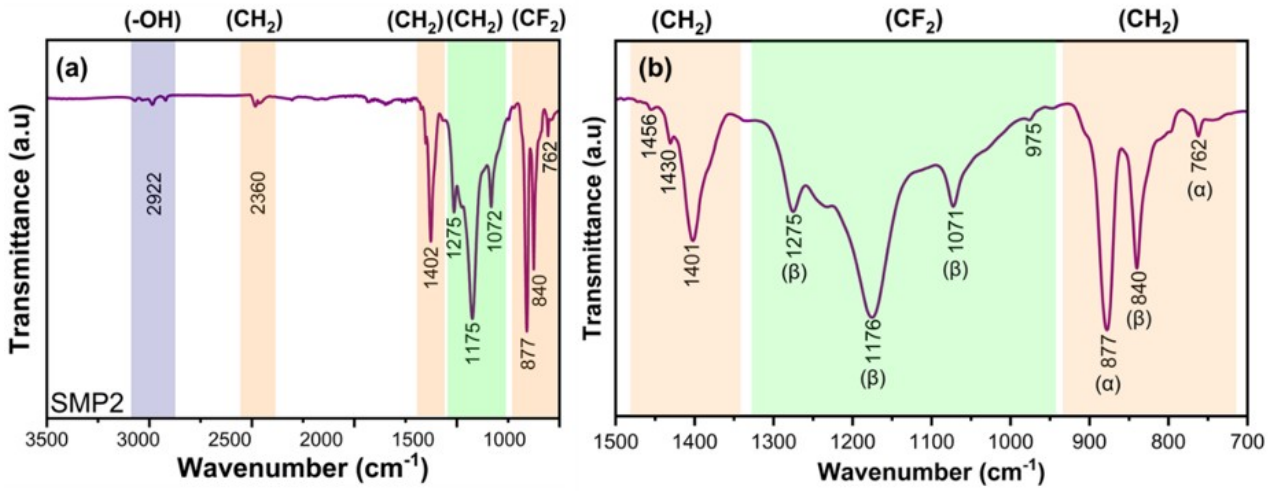

Figure 5. FTIR of the SMP2 (a) 3000-500 (b) 1500-700

crystallization and improves electroactive.

The dominance of β-related band spectroscopy has important implications; β-phase enrichment implies increased dipolar order and crystallinity, which typically correlates with increased mechanical stiffness and dielectric/piezoelectric activity (Edwards et al., 2024). This property can affect the strength of the membrane under hydraulic pressure and its interactions with charged solutes. However, changes in the phase content can also modulate chain packing and free-volume distribution, with potential downstream effects on porosity, water flux, and fouling tendency.

3.5 XRD Analysis of the PVDF Membranes

The XRD Graph, shown in Figure 6, reveals the typical diffraction pattern of PVDF membranes in SMP1 and SMP3 samples, characterized by relatively consistent peak intensities and positions, indicating the presence of a semi-crystalline structure formed during fabrication. The dominant peak appears at around 2θ = 18–20°, which can be attributed to the α-PVDF phase (de Jesus Silva et al., 2020; Suresh et al., 2024), while the peak in the range of 36–40° indicates the presence of the β phase, which is known to have better piezoelectric properties (Ahbab et al., 2025).

However, a more detailed inspection of the diffraction profile reveals the emergence of a strong peak centered at 20–21°, which is widely recognized as the characteristic reflection of the (110)/(200) planes of β-phase PVDF, indicating the formation of a polar crystalline structure. Notably, the intensity of this peak increases significantly from SMP1 (20.14°) to SMP3 (21.44°), suggesting an enhanced fraction and ordering of the β-phase. In contrast, the shoulder peak observed at 18.26–19.36°, corresponding to α-phase reflections, appears relatively weaker, indicating the suppression of non-polar crystalline domains. A semi-quantitative evaluation based on the relative intensity ratio ($I\beta/I\alpha$) demonstrates that SMP3 exhibits a substantially higher β-phase contribution compared to SMP1, confirming the progressive transformation from α- to β-phase under the applied fabrication conditions. This interpretation is consistent with recent study by Roni et al. (2025), where the β-phase is characterized by a dominant diffraction peak at 20.2–20.6°, while α-phase peaks appear at lower angles (17.7–19.9°). Similar enhancement of β-phase intensity due to processing-induced dipole alignment has been reported by Ahmad et al. (2025); Rehman et al. (2025), in PVDF systems subjected to external fields or controlled crystallization conditions. Furthermore, the presence of secondary reflec-

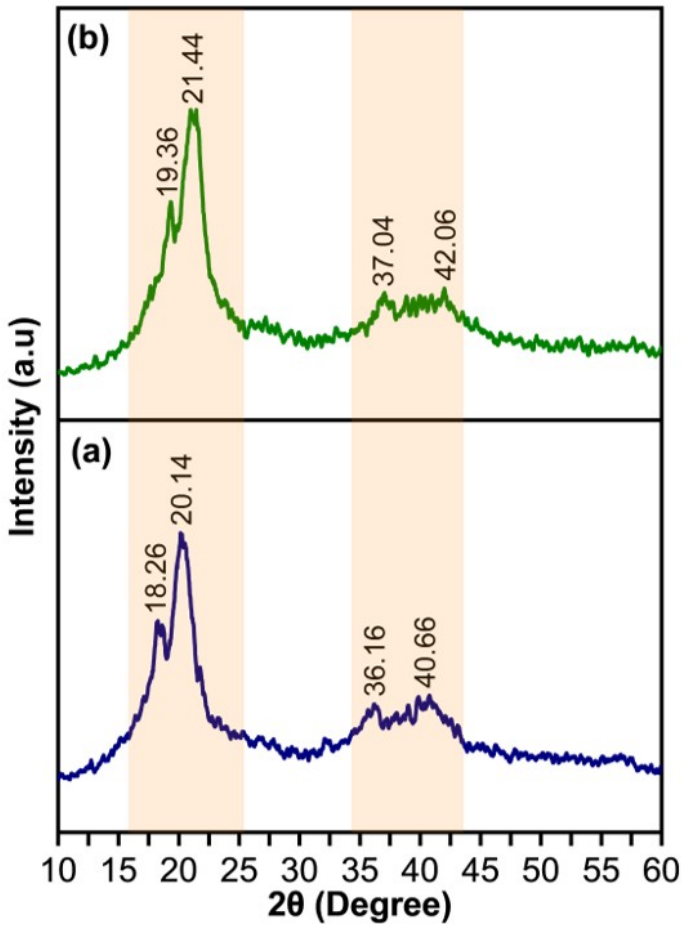

Figure 6. X-Ray Diffaction of the (a) SMP1 and (b) SMP3

tions around 36–42° in the present data can be associated with higher-order crystalline planes or mixed-phase contributions, which are commonly observed in modified PVDF systems with improved structural organization (Nugraha et al., 2024). Additional study by Roopa et al. (2021), also confirm that the attenuation of α-phase peaks accompanied by intensified β-phase reflections indicates successful phase transformation and enhanced crystallinity in PVDF-based materials.

The higher peak intensity in the SMP3 sample compared to that in the SMP1 sample indicates that the increased polymer concentration in the solution contributes to the growth of more regular crystal domains, resulting in a higher degree of crystallinity. This is consistent with the phenomenon whereby a higher polymer content provides more molecular chains to orient under the influence of the applied electric field, thereby strengthening the transition from the amorphous phase to the crystalline phase (Wang et al., 2023). In addition, the differences in intensity between samples also show that the electric field-based fabrication method used in this study not only facilitates pore formation but also affects the distribution of the PVDF crystalline phase. In other words, electric field treatment plays an important role in modifying molecular orientation and phase stability, which ultimately affects the mechanical and functional properties of the membrane (Rothermund et al., 2024). These findings confirm that combining the appropriate polymer concentration with the application of an electric field can be an effective strategy for engineering the crystalline properties of PVDF without the need for additional chemical treatment, thus offering a simpler and more environmentally friendly approach. These findings confirm that combining the right polymer concentration with the application of an electric field can be an effective strategy for engineering the crystalline properties of PVDF without the need for additional chemical treatment, thus offering a simpler and more environmentally friendly approach.

3.6 Water Contact Angle Analysis of the PVDF Membranes

Figure 7 shows the analysis of the water contact angle on PVDF membranes, which provides important information regarding the surface hydrophilicity and its relationship with morphology and filtration performance. In general, the contact angle values decrease over time in all samples, indicating a process of absorption or penetration of water into the membrane structure. SMP1 exhibits the lowest contact angle values, decreasing from 53.706 ± 3.045° to 47.800 ± 1.515°, indicating the most hydrophilic property compared to the other samples. This is consistent with the SEM results, which show that SMP1 has larger pore sizes and a more open structure, allowing water to spread and enter the membrane pores more easily. This behavior can be explained by its relatively large pore size (11.5 μm) and open structure observed in SEM images, which facilitate liquid infiltration into the roporous structure. Such wetting behavior is consistent with the Wenzel model, where the liquid fully wets the roscopically rough surface, increasing the effective solid–liquid contact area and thereby reducing the apparent contact angle. Similar findings have been reported in recent study by Al-Gharabli et al. (2021), where membranes with larger and more open pore structures exhibit enhanced wettability due to capillary-driven penetratio.

In contrast, SMP3 recorded the highest contact angle, decreasing from 70.093 ± 0.579° to 64.127 ± 5.146°, indicating increased hydrophobicity due to its smaller and denser pore structure, as observed in the SEM images. This behavior is attributed to its smaller pore size (5.27 μm) and denser structure, as well as increased surface roughness, confirmed by AFM analysis. The combination of fine pores and higher roughness promotes air entrapment within roscale cavities, leading to the formation of a composite solid–liquid–air interface. This condition is better described by the Cassie–Baxter model, in which the presence of trapped air reduces the effective contact area and increases the apparent contact angle. Similar behavior has been reported in study by Teoh et al. (2021), for structured PVDF membranes exhibiting hierarchical oughness, where air trapping significantly enhances hydrophobicity.

SMP2 falls in between, with intermediate contact angle values ranging from 69.959 ± 2.485° to 66.597 ± 2.864°, reflecting a transitional wetting state governed by both sur-

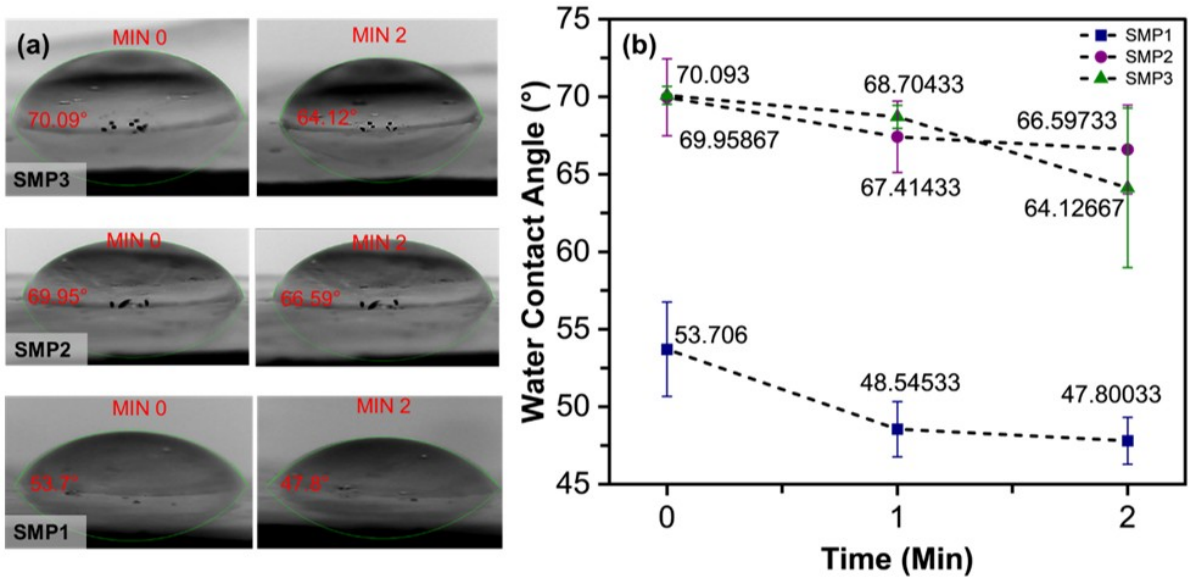

Figure 7. Water Contact Angle of the SMP1, SMP2, and SMP3 (a) Water Droplet (b) Contact Angle

face roughness and partial liquid penetration. This suggests that SMP2 also operates in a mixed Wenzel–Cassie regime, in which water partially infiltrates macropores while retaining trapped air pockets. Such intermediate wetting behavior has been reported in study by Rauter et al. (2021), where this phenomena often associated with complex surface morphologies. This correlation demonstrates that pore size and distribution greatly influence the membrane surface's interaction with water (Hamad et al., 2022). Membranes with larger pores tend to have better wettability, while denser structures hinder water penetration (Zhu and Mao, 2020).

This phenomenon is also consistent with the water flux test results, where SMP1 exhibits the highest flux owing to a combination of hydrophilic properties and an open pore structure, minimizing flow resistance, which will be discussed in the next section. In contrast, SMP3 has the lowest flux owing to its more hydrophobic nature and smaller pore size, which increases resistance to water flow. Thus, these results confirm that there is a strong relationship between membrane morphology (pore size), surface properties (contact angle), and filtration performance (water flux), making the optimization of fabrication parameters key to producing membranes with optimal performance. A comparison of the PVDF membrane contact angles with those in previous studies is presented in Table 3.

The error bars presented in Figure 7 represent the standard deviation of the water contact angle (WCA) measurements obtained from three independent repetitions (n = 3), providing important insights into the surface uniformity and structural heterogeneity of the membranes. SMP1 exhibited a noticeable decrease in standard deviation from ± 3.045° to ± 1.515° over time, indicating that the wetting behavior became more homogeneous as water progressively infiltrated the open pore structure. This trend suggests that capillary-driven penetration reduces local variations in liquid–solid interaction, which is consistent with Wenzel-type wetting behavior on porous surfaces (Al-Gharabli et al., 2021). In contrast, SMP3 showed significantly larger error bars, particularly at longer contact times (up to ± 5.146°), indicating a higher degree of surface heterogeneity. This variability can be attributed to the complex surface morphology and increased roughness observed in the atomic force microscopy (AFM) analysis, which led to spatial variations in local wetting states. Specifically, some regions may retain trapped air and follow Cassie–Baxter behavior, whereas others undergo liquid penetration and transition toward Wenzel wetting. The coexistence of these wetting regimes results in greater dispersion in the measured contact angles. Similar observations have been reported in recent study by Rauter et al. (2021), where heterogeneous porous surfaces exhibit increased variability due to mixed wetting mechanisms. SMP2 demonstrated relatively stable and moderate standard deviation values (± 2.485° to ± 2.864°), suggesting a more uniform surface morphology and consistent wetting behavior across the membrane. This indicates a balanced structural configuration, where pore size distribution and surface roughness are sufficiently homogeneous to minimize local variations in wettability (Rauter et al., 2021). Overall, these results highlight that, beyond average WCA values, the magnitude of the standard deviation plays a crucial role in understanding membrane surface properties. Membranes with higher roughness and more complex pore structures tend to exhibit larger deviations due to localized differences in liquid–solid interactions, emphasizing the importance of considering both mean values and statistical variation in wettability analysis.

Table 3. Comparison of PVDF Membrane Contact Angles with Previous Studies

Membrane Material	Fabrication Methods	Contact Angle (°)	References
PVDF	Membrane Distillation (MD)	157.5	(Hamad et al., 2022)
PVDF	Grafting to	110 – 155	(Hamad et al., 2022)
PVDF-CTFE/SiO_2	Electrospinning	151.3	(Ren et al., 2023)
PVDF	Phase Inversion	130 – 150	(Yang et al., 2023)
PVDF	Electric Field	47 – 60	This Study

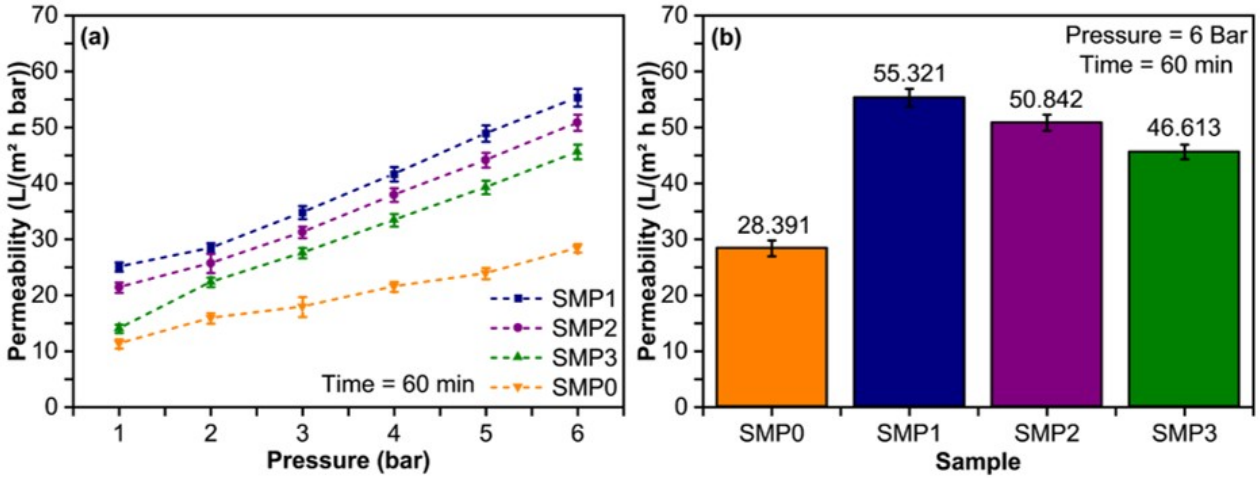

Figure 8. Permeability of the SMP1, SMP2, and SMP3 (a) Water Pressure-Permeability (b) Final Permeability

3.7 Permeability Analysis of the PVDF Membranes

Figure 8 shows the results of the permeability test, indicating that the application of an electric field in the PVDF membrane fabrication process contributes significantly to improved filtration performance. As shown in Figure 8a, the permeability of all samples increased consistently with increasing applied pressure, confirming a typical pressure-driven filtration behavior. At 1 bar, SMP1, SMP2, and SMP3 exhibited flux values of 25.059, 21.374, and 14.004 L/m^2·h·bar, respectively, and these values increased progressively up to 55.321, 50.842, and 45.613 L/m^2·h·bar at 6 bar. Among the samples, SMP1 consistently showed the highest flux across all pressure variations, which was strongly correlated with its morphological characteristics, namely, the presence of larger and more open pore structures, as observed in the SEM analysis. These structural features facilitate easier water transport and reduce flow resistance, thereby allowing for higher permeability. This result confirms that the electric field plays a role in promoting better pore interconnectivity and enhancing fluid transport pathways (Tiwary et al., 2024; Wang et al., 2024). SMP2 demonstrates intermediate performance, with flux values ranging from 21.374 to 50.842 L/m^2·h·bar. This indicates that SMP2 achieves a balance between permeability and structural compactness, where the pore size and distribution are sufficiently optimized to maintain good water transport while improving membrane integrity. Meanwhile, SMP3 consistently exhibits the lowest flux, increasing from 14.004 to 45.613 L/m^2·h·bar as pressure rises. This behavior is in agreement with SEM observations showing smaller and more densely packed pores, which restrict water flow but enhance mechanical strength and structural stability (Firdaus et al., 2025b; Hami et al., 2023).

The observed variation in permeability can be mechanistically explained by the coupled influence of electrostatic forces, pore structure evolution, and polymer concentration. Compared to SMP0 (without electric field), which exhibits significantly lower permeability (28.391 L/m^2·h·bar at 6 bar), the application of an electric field induces electrostatic forces, primarily Coulomb forces and Maxwell stress, that act as driving forces to reorganize polymer chains and promote the formation of interconnected pore channels. This results in the transition from a dense structure (SMP0) to a porous network (SMP1–SMP3), significantly reducing hydraulic resistance and enhancing water transport. Similar enhancements in flux due to electric field-induced structural modification have been reported in study by He et al. (2022), where electric poling or field-assisted fabrication increased permeability by improving pore connectivity and internal alignment. Furthermore, the dependence of permeability on pore size is evident, as larger pores in SMP1 (11.54 μm) yield the highest flux, consistent with study by Khui et al. (2025), showing that permeability increases with pore size and porosity due to reduced flow resistance.

Increasing the PVDF concentration from 25% to 35% led to a reduction in pore size (11.54 μm to 5.27 μm), which conse-

Table 4. Comparison of PVDF Membrane Permeability with Previous Studies

Membrane Material	Fabrication Methods	Water Flux (L/m^2·h·bar)	References
PVDF/Clay-APS	Phase Inversion	~10 ~ ~24	(Pramono et al., 2023)
PVDF	Electrospinning	~9 – 13	(Hu et al., 2022)
PVDF	Phase Inversion	~45	(Ghobadi Moghadam and Hemmati, 2023)
PVDF	Electrospinning	~22 ~ ~35	(Navarro-Tovar et al., 2025)
PVDF/LiCl	Phase Inversion	~17	(Cheng et al., 2022)
PVDF	Electric Field	45.613 – 55.321	This Study

Table 5. Comparison of PVDF Membrane Filtration Performance with Previous Studies

Membrane Material	Fabrication Methods	Rejection Efficiency (%)	References
PVDF/GO	Dip Coating Technique	33.4 – 37.2	(Dawam et al., 2025)
PVDF/p-ATP	Combining nonsolvent-induced phase separation (NIPS) and thermally-induced phase separation (TIPS)	~58 – ~91	(Mao et al., 2023)
PVDF	Phase Inversion	~95	(Reza et al., 2023)
PVDF/LiCl	Phase Inversion	~80	(Cheng et al., 2022)
PVDF/CFTE	Electrospinning	~93	(Ren et al., 2023)
PVDF	Electric Field	~96.72	This Study.

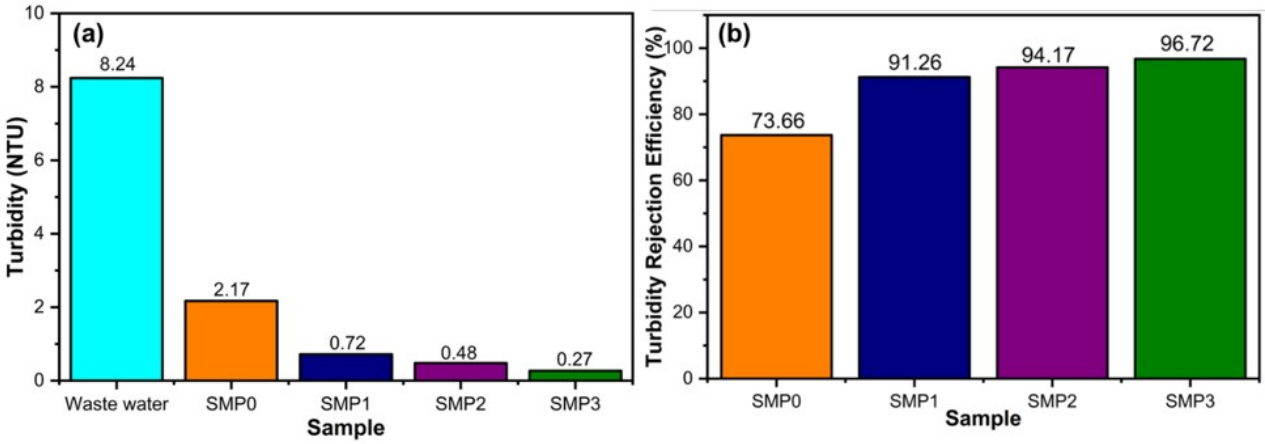

Figure 9. Filtration Performance of the SMP0, SMP1, SMP2, and SMP3 (a) Turbidity (b) Turbidity Rejection Efficiency

quently decreased permeability (55.321 L/m^2·h·bar to 45.613 L/m^2·h·bar). This trend reflects the increasing dominance of viscous and chain entanglement forces at higher polymer concentrations, which act as resisting forces that limit pore growth and reduce effective transport pathways. Similar behavior has been reported in PVDF membranes fabricated via phase inversion study by He et al. (2023), where increased polymer concentration leads to denser structures, smaller pores, and reduced flux. In addition, recent study by Ma et al. (2024), highlight that uniform pore structure and controlled phase separation significantly enhance flux performance, while excessive densification reduces permeability. From a transport perspective, flux is strongly governed by pore geometry and connectivity, where increased pore size and porosity enhance permeability, while increased tortuosity and structural compactness reduce it (Nursiah et al., 2025). Therefore, the results demonstrate a clear mechanistic competition between electrostatic driving forces (electric field) that enhance pore formation and connectivity and viscoelastic resisting forces (polymer concentration) that restrict pore expansion, ultimately determining the final permeability performance. Figure 8b further confirms these findings, showing that at a fixed operating condition (6 bar, 60 min), SMP1 achieved the highest permeability (55.321 L/m^2·h·bar), followed by SMP2 (50.842 L/m^2·h·bar) and SMP3 (45.613 L/m^2·h·bar). The relatively small deviation in the error bars indicates good reproducibility of the membrane performance.

The error bars in the permeability measurements represent the standard deviation of repeated experiments and provide insight into the reproducibility and stability of membrane performance. Overall, all samples exhibited relatively small de-

viations, indicating that the permeability measurements were highly consistent and reliable. SMP1, which showed the highest permeability, also maintained small error bars, suggesting stable flow behavior owing to its open-pore structure and low hydraulic resistance. In contrast, SMP2 and SMP3 exhibited slightly larger deviations, which can be attributed to their more complex and denser pore structures, leading to minor variations in local flow pathways. SMP0 showed low permeability with minimal deviation, indicating a uniformly high resistance structure. These results confirmed that the observed differences in permeability were primarily governed by membrane morphology rather than experimental variability, demonstrating good reproducibility of the filtration performance. Overall, these results highlighted that the electric field influenced not only the membrane surface morphology but also significantly affected pore connectivity and transport efficiency. The ability to achieve high permeability, particularly in SMP1, demonstrated the effectiveness of this method in producing membranes suitable for high-flux filtration applications. However, a trade-off remains evident, where membranes with higher flux tend to have lower mechanical strength, while denser membranes such as SMP3 offer better durability under high-pressure conditions (Dani et al., 2024). Thus, the application of an electric field provided a controllable approach to tailoring membrane performance according to specific filtration requirements. A comparison of the PVDF membrane permeability with previous studies is provided in Table 4.

3.8 Analysis of Turbidity Testing and Membrane Efficiency

As shown in Figure 9ab, the decrease in turbidity from 8.24 NTU (wastewater) to 2.17 NTU (SMP0), 0.72 NTU (SMP1), 0.48 NTU (SMP2), and 0.27 NTU (SMP3) is accompanied by an increase in rejection efficiency from 73.66% to 96.72%, indicating a strong correlation between membrane structure and filtration performance. The SMP0 sample (25% PVDF without an electric field) exhibited the lowest efficiency because of the absence of effective pores, resulting in filtration mechanisms dominated by the solid surface with limited flow pathways. When a 15 kV electric field was applied (SMP1), larger pores (11.54 μm) formed, which significantly increased permeability while enabling size-exclusion filtration and the trapping of suspended particles, resulting in a drastic decrease in turbidity and an efficiency increase to 91.26%. This phenomenon aligns with research conducted by Liu et al. (2025), which found that the formation of controlled porous structures enhances water transport while improving particle retention capacity.

Increasing the PVDF concentration from 25% to 30% and 35% (SMP2 and SMP3) further improved the rejection efficiency to 94.17% and 96.72%, although generally, increasing polymer concentration tends to increase solution viscosity and result in a denser structure. In this context, the combination of an electric field and increased PVDF concentration results in a more homogeneous pore distribution and a more controlled pore network, thereby enhancing the sieving mechanism and reducing particle bypass flow. Recent study by Baroud (2023) indicate that increasing polymer concentration can improve structural density and selectivity without significantly compromising flux, provided that pore morphology remains controlled. In addition, electric fields are known to influence the orientation of polymer chains and the kinetics of phase inversion, resulting in a more ordered pore structure and improving filtration and antifouling performance (Zhang et al., 2025c).

The relationship between pore size and turbidity rejection efficiency is also evident, as pores that are too large can potentially reduce rejection; however, in this system, an increase in PVDF concentration compensates for this effect by forming a denser and more selective structure. This is consistent with study report by Liu et al. (2025), that an increase in pore size and a uniform pore distribution can enhance flux, yet selectivity remains determined by the combination of pore size and total porosity. In general, PVDF membranes are known to achieve turbidity removal efficiencies of over 90% when their pore structure and surface properties are optimized (Al-Tamimi et al., 2025).

Thus, it can be concluded that the electric field plays a key role in pore formation and increased permeability, whereas the PVDF concentration controls the density and selectivity of the membrane structure. The synergy between these two factors results in a membrane with an optimal combination of permeability and rejection capacity, as evidenced by the significant reduction in turbidity and increase in efficiency from SMP0 to SMP3. A comparison of the PVDF membrane filtration performance with those in previous studies is presented in Table 5.

4. CONCLUSIONS

SEM analysis shows that SMP0 (25% PVDF, without an electric field) exhibits a dense, non-porous structure, whereas the application of a 15 kV electric field (SMP1–SMP3) produces well-developed porous morphologies. At 25% PVDF (SMP1), the pores are larger and less uniform (11.54 μm), whereas increasing the concentration to 35% (SMP3) results in smaller and more homogeneous pores (5.27 μm), indicating improved structural control. AFM analysis confirms relatively smooth surfaces, although SMP1 shows larger surface features (>2 μm) compared to SMP3 (<1 μm), suggesting that a higher PVDF concentration refines the surface morphology without reducing the smoothness. This densification is correlated with improved mechanical properties. The tensile strength increases from 12.28 MPa (SMP0) to 43.21 MPa (SMP3), while Young's modulus reaches 780 MPa, indicating enhanced membrane strength and rigidity. FTIR analysis reveals that the electric field promotes β-phase formation, especially in SMP2, enhancing chain alignment and polarization. XRD results further confirm increased crystallinity in the treated membranes. Water contact angle measurements indicate a slightly reduced hydrophilicity with increasing PVDF concentration owing to a more compact structure. In terms of filtration performance, permeability improves significantly with the application of an

electric field, with SMP1 achieving the highest value (55.32 L/m^2·h·bar), while SMP3 offers a better balance between permeability and selectivity. Turbidity rejection exceeds 90% (91.26–96.72%) for SMP1-SMP3, compared to 73.66% for SMP0. Overall, this method enables precise morphology control, enhances β-phase formation, improves performance, and these membranes show strong potential as composite base materials; however, stability and fouling studies remain necessary.

5. ACKNOWLEDGMENT

The research of this article was funded by Directorate of Research and Community Service Directorate General of Research and Development Ministry of Higher Education, Science and Technology In accordance with the Contract for the Implementation of the State University Operational Assistance Program Research Program Number: 109/C3/DT.05.00/PL/2025.

REFERENCES

Acarer-Arat, S., M. Tufekci, i. Pir, and N. Tufekci (2024). Nanocellulose in Polyvinylidene Fluoride (PVDF) Membranes: Assessing Reinforcement Impact and Modelling Techniques. *Journal of Environmental Chemical Engineering*, **12**(6); 114749

Ahbab, N., S. Naz, T.-B. Xu, and S. Zhang (2025). A Comprehensive Review of Piezoelectric PVDF Polymer Fabrications and Characteristics. *Micromachines*, **16**(4); 386

Ahmad, S., M. Zakria, B. Khanam, T. M. Khan, M. Raffi, S. Ullah, and J. Feng (2025). Enhanced Piezoelectric Properties of Electrospun PVDF Nanofibers by Integration of ZnO and MgZnO Nanoparticles. *Next Materials*, **9**; 101303

Ahmadi Bonakdar, M. and D. Rodrigue (2024). Electrospinning: Processes, Structures, and Materials. *Macromol*, **4**; 58–103

Al-Gharabli, S., Z. Abu El-Rub, E. Hamad, W. Kujawski, Z. Flanc, K. Pianka, and J. Kujawa (2021). Surfaces with Adjustable Features—Effective and Durable Materials for Water Desalination. *International Journal of Molecular Sciences*, **22**(21); 11743

Al-Tamimi, N. J., A. F. Al-Alawy, and M. Al-Shaeli (2025). Evaluation of Microfiltration and Ultrafiltration Membranes for Improving Water Quality: Removal of Turbidity, Suspended Solids, and Bacteria from the Tigris River. *Iraqi Journal of Chemical and Petroleum Engineering*, **26**(1); 23–34

Albiladi, A., L. Gzara, H. Organji, N. S. Alkayal, and A. Figoli (2023). Electrospun Poly (Vinylidene Fluoride-Co-Hexafluoropropylene) Nanofiber Membranes for Brine Treatment via Membrane Distillation. *Polymers*, **15**(12); 2706

Almafie, M. R., R. Dani, Riyanto, L. Marlina, J. Jauhari, and I. Sriyanti (2024). Preparation of PAN/PVDF Nanofiber Mats Loaded with Coconut Shell Activated Carbon and Silicon Dioxide for Lithium-Ion Battery Anodes. *Science and Technology Indonesia*, **9**(2); 427–447

Almafie, M. R., A. Fudholi, R. Dani, M. K. N. A. P. Idjan, I. Royani, and I. Sriyanti (2025). Effects of Electrospinning Parameters on Polycaprolactone Membrane Diameter: An Investigation Utilizing Central Composite Design and Characterization. *Results in Engineering*, **25**; 104002

Amin, N. A. A. M., M. A. Mokhter, N. Salamun, M. F. b. Mohamad, and W. M. A. W. Mahmood (2023). Anti-Fouling Electrospun Organic and Inorganic Nanofiber Membranes for Wastewater Treatment. *South African Journal of Chemical Engineering*, **44**; 302–317

Annadurai, A. and M. S. Alam (2025). Physicochemical, Thermal, and Surface Behavior of Fatliquors and Their Applications in Leather Processing and Sustainability. *Journal of Chemical & Engineering Data*, **70**(5); 1783–1800

Arif, Z., N. K. Sethy, L. Kumari, P. K. Mishra, and B. Verma (2019). Antifouling Behaviour of PVDF/TiO2 Composite Membrane: A Quantitative and Qualitative Assessment. *Iranian Polymer Journal*, **28**(4); 301–312

Baroud, T. N. (2023). Tuning PVDF Membrane Porosity and Wettability Resistance via Varying Substrate Morphology for the Desalination of Highly Saline Water. *Membranes*, **13**(4); 395

Basko, A., T. Lebedeva, M. Yurov, A. Ilyasova, G. Elyashevich, V. Lavrentyev, and K. Pochivalov (2023). Mechanism of PVDF Membrane Formation by NIPS Revisited: Effect of Precipitation Bath Nature and Polymer–Solvent Affinity. *Polymers*, **15**(21); 4307

Bertolini, M. C., N. Zamperlin, G. M. Barra, and A. Pegoretti (2023). Development of Poly (Vinylidene Fluoride)/Thermoplastic Polyurethane/Carbon Black-polypyrrole Composites with Enhanced Piezoelectric Properties. *SPE Polymers*, **4**(4); 143–155

Besghini, D., M. Mauri, and R. Simonutti (2019). Time Domain NMR in Polymer Science: From the Laboratory to the Industry. *Applied Sciences*, **9**(9); 1801

Bohr, S. J., F. Wang, M. Metze, J. L. Vukušić, A. Sapalidis, M. Ulbricht, and S. Barbe (2023). State-of-the-Art Review of Porous Polymer Membrane Formation Characterization—How Numerical and Experimental Approaches Dovetail to Drive Innovation. *Frontiers in Sustainability*, **4**; 1093911

Chen, F., J. Li, Y. Shi, H. Ye, Y. Zhou, Y. Zhao, and J. Xu (2024a). Effect of Stretching Orientation on the Crystalline Structure and Energy Storage Properties of Poly(vinylidene Fluoride) Films. *Materials Today Communications*, **41**; 110598

Chen, M., S. G. J. Heijman, and L. C. Rietveld (2024b). Ceramic Membrane Filtration for Oily Wastewater Treatment: Basics, Membrane Fouling and Fouling Control. *Desalination*, **583**; 117727

Cheng, L., Z. Zhou, L. Li, P. Xiao, Y. Ma, F. Liu, and J. Li (2022). PVDF/MOFs Mixed Matrix Ultrafiltration Membrane for Efficient Water Treatment. *Frontiers in Chemistry*, **10**; 985750

Choi, S., B. Kang, E. Yang, K. Kim, M. K. Kwak, P. S. Chang,

and H. S. Jung (2023). Precise Control of Liposome Size Using Characteristic Time Depends on Solvent Type and Membrane Properties. *Scientific Reports*, **13**(1); 1–12

Dani, R., M. R. Almafie, A. Mataram, M. D. P. Lamura, H. Akhsan, L. Marlina, and I. Sriyanti (2026). Preparation of Polyacrylonitrile-Polyethersulfone Nanofibers Loaded with Reduced Graphene Oxide from Palm Kernel Shell for Wastewater Filtration. *Science and Technology Indonesia*, **11**(2); 457–480

Dani, R., Ismet, L. Marlina, R. Alisya, M. A. K. Aldi, A. Ludian-Syah, and I. Sriyanti (2024). Synthesis of Activated Carbon from Coconut Shell and Recycled Styrofoam Nanofiber for Water Filtration. *Makara Journal of Science*, **28**(4); 357–369

Dawam, M., F. M. El-Sayed, M. Y. Zorainy, H. Oraby, and M. Gobara (2025). Enhancement of PVDF Membranes Using Graphene Oxide Nanoparticles and Polyvinyl Alcohol for Water Purification Applications. *Scientific Reports*, **15**(1); 39759

de Jesus Silva, A. J., M. M. Contreras, C. R. Nascimento, and M. F. da Costa (2020). Kinetics of Thermal Degradation and Lifetime Study of Poly(vinylidene Fluoride) (PVDF) Subjected to Bioethanol Fuel Accelerated Aging. *Heliyon*, **6**(7); e04573

Edwards, T. R., R. Shankar, P. G. H. Smith, J. A. Cross, Z. A. B. Lequeux, L. K. Kemp, and S. E. Morgan (2024). Beta-Phase Crystallinity, Printability, and Piezoelectric Characteristics of Polyvinylidene Fluoride (PVDF)/Poly(methyl Methacrylate) (PMMA)/Cyclopentyl-Polyhedral Oligomeric Silsesquioxane (Cp-POSS) Melt-Compounded Blends. *ACS Applied Polymer Materials*, **6**(10); 5803–5813

Eniola, J. O., J. Kujawa, A. Nwokoye, S. Al-Gharabli, A. K. Avornyo, A. Giwa, and J. A. Okolie (2024). Advances in Electrochemical Membranes for Water Treatment: A Comprehensive Review. *Desalination and Water Treatment*, **319**; 100450

Fakhry, M., O. Soppera, and D. Berling (2025). Innovative Elaboration of Polyvinylidene Fluoride Thin Films via Dip-Coating: Beta Phase Optimization, Humidity Control, Nanoparticles Addition, and Topographic Analysis. *Micro*, **5**(1); 12

Firdaus, A., R. Dani, M. S. P. Gantada, A. F. Ismail, N. Nukman, I. Bizzy, and A. Mataram (2025a). Identifying the Features of Mechanical and Physicochemical Characteristics of Polyethersulfone Membranes Using Electric Field Method for Water Filtration Applications. *Eastern-European Journal of Enterprise Technologies*, **6**(138); 14–27

Firdaus, A., S. Nasir, R. Dani, I. N. Prasatya, A. F. Ismail, M. H. D. Othman, and A. Mataram (2025b). Synthesis of Polyethersulfone Membranes With the Addition of Silver Nitrate for Water Filter Applications. *EUREKA, Physics and Engineering*, **2025**(1); 121–131

Fu, W., H. Lu, B. Li, S. Yang, and W. Su (2025). Mechanical-Dielectric Synergistic Modulation Enables High Energy Density in TPU/PVDF All-Organic Films. *Journal of Applied Polymer Science*, **142**(47); e57838

Gayatri, R., A. N. S. Fizal, E. Yuliwati, M. Z. Zailani, J. Jaafar, M. S. Hossain, and A. N. Ahmad Yahaya (2024). Effect of Polyvinylidene Fluoride Concentration in PVDF-TiO_2-PVP Composite Membranes Properties and Its Performance in Bovine Serum Albumin Rejection. *Case Studies in Chemical and Environmental Engineering*, **9**; 100620

Ghobadi Moghadam, A. and A. Hemmati (2023). Improved Water Purification by PVDF Ultrafiltration Membrane Modified With GO-PVA-NaAlg Hydrogel. *Scientific Reports*, **13**(1); 8076

Ghorbandoust, M., M. Fasihi, and R. Norouzbeigi (2024). Tuning Pore Size and Density of Rigid Polylactic Acid Foams Through Thermally Induced Phase Separation and Optimization Using Response Surface Methodology. *Scientific Reports*, **14**(1); 1–21

Hamad, E. M., S. Al-Gharabli, and J. Kujawa (2022). Tunable Hydrophobicity and Roughness on PVDF Surface by Grafting to Mode – Approach to Enhance Membrane Performance in Membrane Distillation Process. *Separation and Purification Technology*, **291**; 120935

Hami, S. S. B. M., N. D. N. Affandi, L. Indrie, S. Tripa, A. M. Harun, and M. R. Ahmad (2023). Enhancing Mechanical Properties and Flux of Nanofibre Membranes for Water Filtration. *Polymers*, **15**(15); 3281

Hamta, A., F. Zokaee Ashtiani, M. Karimi, and A. Safikhani (2021). Manipulating of Polyacrylonitrile Membrane Porosity via SiO_2 and TiO_2 Nanoparticles: Thermodynamic and Experimental Point of View. *Polymers for Advanced Technologies*, **32**(2); 872–885

He, T., X. Li, Q. Wang, Y. Zhou, X. Wang, Z. Wang, and Z. Cui (2022). Poly(vinylidene Fluoride) (PVDF) Membrane Fabrication With an Ionic Liquid via Non-Solvent Thermally Induced Phase Separation (N-TIPs). *Applied Water Science*, **12**(3); 42

He, W., S. Fan, G. Liu, L. Zhou, L. Chai, H. Zhu, and B. Yu (2023). Preparation and Properties of Poly (Vinylidene Fluoride) Membrane With Inverse Opal-Like Structure. *Separation and Purification Technology*, **306**; 122446

Hu, H.-W., H.-K. Tsao, and Y.-J. Sheng (2024). Impact of Nonsolvent–Solvent Affinity on Membrane Morphology and Microstructure: Unraveling the Transition From Traversing Pore to Closed Void Structures. *Macromolecules*, **57**(15); 7640–7653

Hu, X., X. Chen, M. Giagnorio, C. Wu, Y. Luo, C. Hélix-Nielsen, and W. Zhang (2022). Beaded Electrospun Polyvinylidene Fluoride (PVDF) Membranes for Membrane Distillation (MD). *Journal of Membrane Science*, **661**; 120850

Huang, Y.-H., S. Seenuvasan, M.-J. Wang, and T.-S. Chung (2025). Effects of Polyvinylidene Difluoride (PVDF) Molecular Weight on Hydrophobic Membranes Prepared by the Plasma Assisted Nonsolvent Induced Phase Separation (PA-NIPS) Method. *Chemical Engineering Journal*, **505**; 159147

Huang, Y.-H., M.-J. Wang, and T.-S. Chung (2024). Development of Multifunctional Membranes via Plasma-Assisted

Nonsolvent Induced Phase Separation. *Nature Communications*, **15**(1); 1092

Islam, M. D., F. J. Uddin, T. U. Rashid, and M. Shahruzzaman (2023). Cellulose Acetate-Based Membrane for Wastewater Treatment—A State-of-the-Art Review. *Materials Advances*, **4**(18); 4054–4102

Jayasekara, A. S. and P. Cebe (2023). Quantitative Analysis of Polar Crystalline Fractions in Poly(vinylidene Fluoride) Electrospun Fibers and Electrosprayed Films. *Polymer*, **281**; 126140

Kariuki, R., R. Penman, S. J. Bryant, R. Orrell-Trigg, N. Meftahi, R. J. Crawford, and A. Elbourne (2022). Behavior of Citrate-Capped Ultrasmall Gold Nanoparticles on a Supported Lipid Bilayer Interface at Atomic Resolution. *ACS Nano*, **16**(10); 17179–17196

Ke, G., X. Jin, and H. Hu (2020). Electrospun Polyvinylidene Fluoride/Polyacrylonitrile Composite Fibers: Fabrication and Characterization. *Iranian Polymer Journal (English Edition)*, **29**(1); 37–46

Khui, P. L. N., M. R. Rahman, K. A. b. M. Said, M. Namakka, M. Shahabuddin, M. S. M. Al-Saleem, and M. M. Rahman (2025). Enhanced Flux and Surface Modification of PVDF Hollow Fiber Membranes Using Bamboo Cellulose/PVA Composite Coatings. *Polymer Bulletin*, **82**(18); 12909–12927

Kim, S. Y., S. Kim, and C. Park (2025). Evaluation of Ceramic Membrane Filtration for Alternatives to Microplastics in Cosmetic Formulations Using FlowCam Analysis. *Membranes*, **15**(1); 35

Liu, R., J. Yang, R. Zhang, H. Li, and R. Mu (2025). Performance Comparison of Nano-Al2O3-Modified PVDF Membranes Fabricated via Two Methods for Enhanced Dye Removal. *RSC Advances*, **15**(6); 4163–4172

Ma, Y., X. Zhao, and B. He (2024). Fabrication of Nanoparticle Array Membranes by Integrating Semi-Crystalline Polymer Self-Assembly With NIPS for Water Treatment. *Nanoscale Advances*, **6**(14); 3543–3552

Mao, H., S. Zhou, M. Li, R. Wang, Z. Ma, H. Xiao, and C. Chen (2023). PVDF Ultrafiltration Membrane With Enhanced Mechanical and Filtration Performance by Hydrophilic pH-Response Nanofibers Modification. *Separation and Purification Technology*, **314**; 123613

Marshall, J. E., A. Zhenova, S. Roberts, T. Petchey, P. Zhu, C. E. J. Dancer, and V. Goodship (2021). On the Solubility and Stability of Polyvinylidene Fluoride. *Polymers*, **13**(9); 1354

Mataram, A., A. Firdaus, M. Yanis, R. Dani, S. Nasir, A. F. Ismail, and M. H. D. Othman (2024). Synthesis of Polyethersulfone/Titanium Dioxide Membranes: Analysis of Morphology, Mechanical Properties, and Water Filtration Performance. *Eastern-European Journal of Enterprise Technologies*, **6**(6(132)); 16–25

Nagandran, S., P. S. Goh, A. F. Ismail, T.-W. Wong, and W. R. Binti Wan Dagang (2020). The Recent Progress in Modification of Polymeric Membranes Using Organic Macromolecules for Water Treatment. *Symmetry*, **12**(2); 239

Navarro-Tovar, R., B. Qiu, P. Martin, P. Gorgojo, and M. Perez-Page (2025). Advanced Desalination Performance Using PVDF Electrospun Nanofiber Membranes Across Multiple Membrane Distillation Configuration. *Desalination*, **598**; 118425

Nawaz, H., M. Umar, A. Ullah, H. Razzaq, K. M. Zia, and X. Liu (2021). Polyvinylidene Fluoride Nanocomposite Super Hydrophilic Membrane Integrated With Polyaniline-Graphene Oxide Nano Fillers for Treatment of Textile Effluents. *Journal of Hazardous Materials*, **403**; 123587

Nazari, S. and A. Abdelrasoul (2022). Impact of Membrane Modification and Surface Immobilization Techniques on the Hemocompatibility of Hemodialysis Membranes: A Critical Review. *Membranes*, **12**(11); 1063

Nugraha, A. S., C. C. Chou, and B. B. Aji (2024). Local Analysis of Crystalline Phases and Properties of Poly(vinylidene Fluoride) Electrospun Composites With $BaTiO_3$ Nanorods. *Polymer International*, **73**(2); 119–129

Nursiah, K., S. J. Bohr, L. K. Atfane, S. Cerneaux, S. Barbe, and M. D. Barboiu (2025). PVDF Membranes for Membrane Distillation Prepared by VIPS – A Combined Study of Artificial Water Channel Effectiveness and Membrane Performance Prediction. *Open Research Europe*, **4**; 102

Ohno, S., I. Nakata, R. Nagumo, K. Akamatsu, X. Wang, and S. Nakao (2021). Development of Low-Fouling PVDF Membranes Blended With Poly(2-Methoxyethyl Acrylate) via NIPS Process. *Separation and Purification Technology*, **276**; 119331

Osama, L., H. T. Handal, S. A. M. El-Sayed, E. M. Elzayat, and M. Mabrouk (2024). Fabrication and Optimisation of Alumina Nanoporous Membranes for Drug Delivery Applications: A Comparative Study. *Nanomaterials*, **14**(13); 1078

Pramono, E., G. P. W. Sejati, S. Wahyuningsih, and C. Purnawan (2023). Polyvinylidene Fluoride (PVDF)/Modified Clay Hybrid Membrane for Humic Acid and Methylene Blue Filtration. *Indonesian Journal of Chemistry*, **23**(2); 425

Qiao, J., H. Mu, C. Liu, and Z. Liu (2023). Magnetic Field Effects on the Structure, Dielectric and Energy Storage Properties of High-Entropy Spinel Ferrite ($La_{0\cdot14}Ce_{0\cdot14}Mn_{0\cdot14}Zr_{0\cdot14}Cu_{0\cdot14}Ca_{0\cdot14}Ni_{0\cdot14}$)$Fe_2O_4$/ PVDF Nanocomposites. *Polymers*, **15**(8); 1842

Qua, M. S., Y. Zhao, J. Zhang, S. Hernandez, A. T. Paing, K. Mottaiyan, and C. Gudipati (2022). Novel Sandwich-Structured Hollow Fiber Membrane for High-Efficiency Membrane Distillation and Scale-Up for Pilot Validation. *Membranes*, **12**; 423

Rauter, M. T., S. K. Schnell, and S. Kjelstrup (2021). Cassie–Baxter and Wenzel States and the Effect of Interfaces on Transport Properties Across Membranes. *The Journal of Physical Chemistry B*, **125**(46); 12730–12740

Rehman, Z. U., Farhan, S. Ahmad, H. Ullah, S. A. Alqarni, S. Yao, and M. E. A. Zaki (2025). Thermal and Electri-

cal Properties of PVDF Modified Co_3/O_4 Functionalized MWCNTs. *RSC Advances*, **15**(11); 8740–8749

Ren, W., J. Pan, W. Gai, X. Pan, H. Chen, J. Li, and L. Huang (2023). Fabrication and Characterization of PVDF-CTFE/SiO2 Electrospun Nanofibrous Membranes With Micro and Nano-Rough Structures for Efficient Oil-Water Separation. *Separation and Purification Technology*, **311**; 123228

Reza, M., E. Pramono, and C. L. Radiman (2023). Improving Separation Performance of PVDF Ultrafiltration Membranes by Blending with Cellulose Acetate. *Iranian Journal of Chemistry and Chemical Engineering*, **42**(3); 1017–1029

Roni, M. N. P., T. A. Neshath, M. A. Hakim, M. M. Hasan, M. H. Rahman, M. S. Hossan, and M. H. Khatun (2025). Optimizing Beta-Phase Content in PVDF Membranes via Modification of Dope Solution With Citric Acid/Nano-TiO2 Using Nonsolvent-Induced Phase Separation Method. *Polymers*, **17**(4); 481

Roopa, T., H. N. Murthy, D. Harish, A. Jain, and G. Angadi (2021). Properties of PVDF Films Stretched in Machine Direction. *Polymers and Polymer Composites*, **29**(3); 198–206

Rothermund, M. A., S. J. Koehler, and V. Vaissier Welborn (2024). Electric Fields in Polymeric Systems. *Chemical Reviews*, **124**(23); 13331–13369

Silva, J. A. S. G. d., W. R. d. Silva Júnior, A. N. R. d. Silva, R. Künzel, J. R. R. Bortoleto, E. B. d. Melo, and N. M. Trindade (2023). Structural Characterization of Polymeric Nanofibers of Polyvinylidene Fluoride (PVDF). *Polímeros*, **33**(1); e20230011

Sisay, E. J., A. N. Al-Tayawi, Z. László, and S. Kertész (2023). Recent Advances in Organic Fouling Control and Mitigation Strategies in Membrane Separation Processes: A Review. *Sustainability*, **15**(18); 13389

Sriyanti, I., M. R. Almafie, M. K. Nuha Ap Idjan, R. Dani, I. Solihah, E. Syafri, and L. Marlina (2025). Electrospun Nanofiber Membrane of Piper Beetle Loaded PVDF/PAN for Medical Mask Applications: Psychochemical Characteristics, Antibacterial and Air Filter Test. *Advanced Membranes*, *5*; 100149

Sriyanti, I., R. Dani, M. R. Almafie, R. U. Partan, M. K. N. Ap Idjan, and L. Marlina (2024a). Optimization of Diameter and Mechanical Properties of Polyacrylonitrile/Polyvinylidene Fluoride/Graphene Oxide Coconut Shell Composite Nanofiber Mats Using Response Surface Methodology. *Case Studies in Chemical and Environmental Engineering*, **10**; 101030

Sriyanti, I., R. F. Ramadhani, M. R. Almafie, M. K. N. Ap Idjan, E. Syafri, I. Solihah, and A. Fudholi (2024b). Physicochemical and Mechanical Properties of Polyvinylidene Fluoride Nanofiber Membranes. *Case Studies in Chemical and Environmental Engineering*, **9**; 100588

Sultana, S., D. Chakraborty, M. A. Parvez, M. R. Chandan, and M. Rahaman (2025). Polymeric Membranes for Advanced Separation and Sensing: Materials and Mechanisms for Emerging Applications–A Review. *Chemistry – An Asian Journal*, **20**(18); e00714

Suresh, S., T. Nabiyeva, L. Biniek, and E. B. Gowd (2024). Poly(vinylidene Fluoride) Aerogels With Alpha, Beta, and Gamma Crystalline Forms: Correlating Physicochemical Properties With Polymorphic Structures. *ACS Polymers Au*, **4**(2); 128–139

Tansel, T. (2021). Effect of Electric Field Assisted Crystallisation of PVDF-TrFE and Their Functional Properties. *Sensors and Actuators A: Physical*, **332**; 113059

Teoh, G. H., B. S. Ooi, Z. A. Jawad, and S. C. Low (2021). Impacts of PVDF Polymorphism and Surface Printing Micro-Roughness on Superhydrophobic Membrane to Desalinate High Saline Water. *Journal of Environmental Chemical Engineering*, **9**(4); 105418

Thakur, V. N. and J. I. Han (2022). Combined Triboelectric and Piezoelectric Effect in ZnO/PVDF Hybrid-Based Fiber-Structured Nanogenerator With PDMS:Carbon Black Electrodes. *Polymers*, **14**(20); 4414

Tiwary, S. K., M. Singh, S. V. Chavan, and A. Karim (2024). Graphene Oxide-Based Membranes for Water Desalination and Purification. *NPJ 2D Materials and Applications*, **8**(1); 27

Wang, J., S. C. Abbas, L. Li, C. C. Walker, Y. Ni, and Z. Cai (2024). Cellulose Membranes: Synthesis and Applications for Water and Gas Separation and Purification. *Membranes*, **14**(7); 148

Wang, L., C. Yang, X. Wang, J. Shen, W. Sun, J. Wang, and Z. Wang (2023). Advances in Polymers and Composite Dielectrics for Thermal Transport and High-Temperature Applications. *Composites Part A: Applied Science and Manufacturing*, **164**; 107320

Yang, D., Y. Yang, T. Wong, S. Iguodala, A. Wang, L. Lovell, and Q. Song (2025). Solution-Processable Polymer Membranes With Hydrophilic Subnanometre Pores for Sustainable Lithium Extraction. *Nature Water*, **3**(3); 319–333

Yang, J., W. Sun, J. Ju, Y. Tan, and H. Yuan (2023). Facile Fabrication of Superwetting PVDF Membrane for Highly Efficient Oil/Water Separation. *Polymers*, **15**(2); 327.

Zaitzeff, M. J. and L. J. Groven (2023). Crash Precipitation of Nanoscale Beta-Phase PVDF Particles. *Materials Letters*, **330**; 133221

Zhang, H., Q. Wang, J. Yin, Y. Gao, X. Zhang, Q. Zhou, and Z. Cui (2025a). Evolution of Piezoelectric PVDF Membrane for Energy Transducer and Membrane Distillation. *Chemical Engineering Journal*, **524**; 169672

Zhang, L., S. Li, Z. Zhu, G. Rui, B. Du, D. Chen, and L. Zhu (2023). Recent Progress on Structure Manipulation of Poly(vinylidene Fluoride)-Based Ferroelectric Polymers for Enhanced Piezoelectricity and Applications. *Advanced Functional Materials*, **33**(38); 2301302

Zhang, N., X. Dong, S. He, Z. Liang, W. Li, Q. Qian, and C. Jiang (2025b). Ultra-High Electrostriction and Ferroelectricity in Poly (Vinylidene Fluoride) by 'Printing of Charge' Throughout the Film. *Nature Communications*, **16**(1); 744

Zhang, X., Y. Liao, and A. Ghani Razaqpur (2024). Electrospinning-Based Super Liquid-Repellent Membranes

for Membrane Distillation: Theory, Fabrications, Applications, and Challenges. In *Electrospinning - Theory, Applications, and Update Challenges*. IntechOpen. Electrospinning-Theory, Applications, and Update Challenges

Zhang, Y., J. Xing, G. Wei, L. Rao, G. He, H. Du, and X. Quan (2025c). Advanced Electrically Conductive Carbon Nanotubes-PVDF Composite Membranes With Electro-Promoted Water Treatment Performance. *Nature Communications*, **16**(1); 11419

Zhu, M. and Y. Mao (2020). Large-Pore-Size Membranes Tuned by Chemically Vapor Deposited Nanocoatings for Rapid and Controlled Desalination. *RSC Advances*, **10**(66); 40562–40568

